5. Discussion

This section provides an overview of the existing crack growth data for Ni-base weld alloys and discusses in this context the data generated at ANL.

5.1 Cyclic Crack Growth Rates

5.1.1 Air Environment

The fatigue CGR (da/dN) data on Ni–alloy welds in air are quite limited.[47–51] Most of the tests have been conducted on Alloy 182 and some on Alloy 52. The results indicate that the effect of temperature on CGRs of the weld metals is similar to that for Alloy 600. Fatigue crack growth data for Alloys 82 and 152 in air are not available. The experimental CGRs obtained under cyclic loading for Alloys 52 and 182 and those predicted in air for Alloy 600 under the same loading conditions are plotted in Fig. 55. In general, the CGRs for Ni–alloy welds are a factor of ≈2 higher (dashed line) than for Alloy 600 under the same loading conditions. Because so few data are available, comparisons of the results for the weld alloys are usually made in terms of the results for Alloy 600 in air, rather than the weld alloys in air.

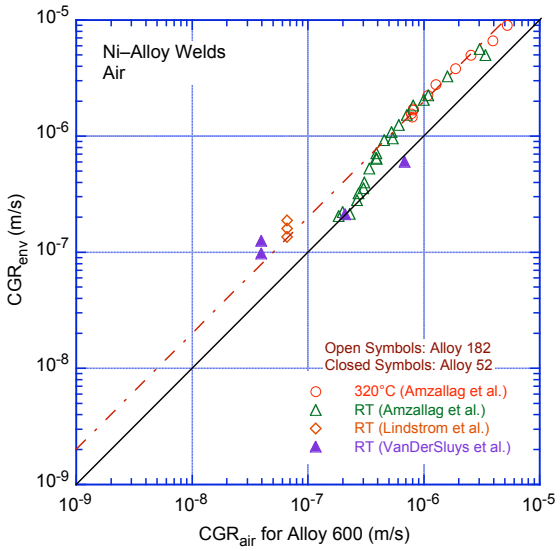

Figure 55.
Experimental values of fatigue crack growth rate of Alloys 182 and 52 in air as a function of those estimated for Alloy 600 under the same loading conditions. Data obtained by Linstrom et al. (Ref. 47), Amzallag et al. (Ref. 48), and Van Der Sluys et al. (Ref. 49).

5.1.2 PWR Environment

The fatigue CGR data on Ni–alloy welds in simulated PWR environments are available from ≈120 tests conducted on Alloys 182, 82, 152, and 52 at 243–345°C.[47,48–51] The loading conditions for these tests include R = 0.1–0.75, K_{max} = 20–100 MPa·$m^{1/2}$, and rise time = 0.5–5000 s. The results indicate very little effect of PWR environment on the fatigue CGRs of Ni–alloy weld metals. However, only about 10% of the data were obtained under conditions for which significant environmental enhancement would be expected.

The experimental CGRs obtained by Van Der Sluys et al.[49] for Alloy 82 and by James and Mills[51] for Alloy 182 are plotted in Fig. 56 as a function of the CGRs predicted for Alloy 600 in air under the same loading conditions. The James and Mills[51] data are for 243°C, where environmental effects would

be expected to be small. Most of the data were obtained under loading conditions that result in CGRs greater than 1 x 10^{-9} m/s in air, i.e., load ratios ≤0.2 and rise times ≤10 s. Under these loading conditions, crack growth is primarily controlled by mechanical fatigue, and environmental effects are not expected to be significant even in materials susceptible to environmental enhancement. The data for Alloy 82 (Fig. 56a) extend into a loading region where strain-rate-dependent environmental enhancement would be expected in susceptible materials, although there are only a few data in the region where significant enhancement would be expected. The available data show very little frequency–dependent environmental enhancement and are best represented by the expression

$$CGR_{env} = CGR_{air\ A600} + 0.12\ (CGR_{air\ A600})^{0.82}, \quad (11)$$

where $CGR_{air\ A600}$ is the growth rate predicted for Alloy 600 in air under the same loading conditions, although a simple constant multiplier would also represent the data almost as well.

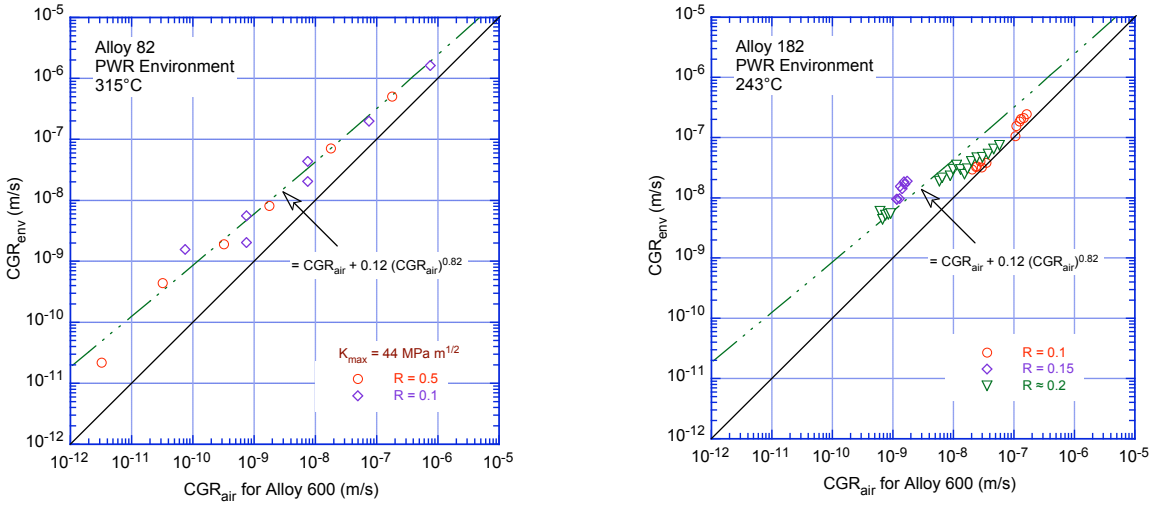

(a) (b)

Figure 56. Fatigue CGR data for (a) Alloy 82 and (b) Alloy 182 weld metal in PWR environment as a function of the growth rate for Alloy 600 in air under the same loading conditions. Data obtained by VanDerSluys et al. (Ref. 49) and James and Mills (Ref. 51).

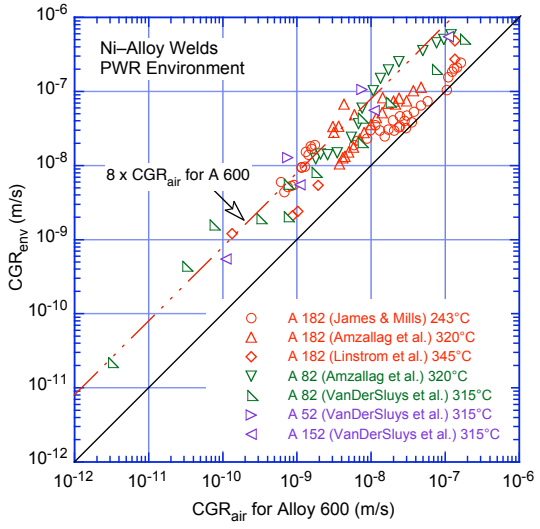

Figure 57.
Fatigue CGR data for Ni–alloy welds in PWR environment as a function of the growth rate for Alloy 600 in air under the same loading conditions. Data from Refs. 47–51.

Literature data on fatigue CGR for Ni–alloy welds in the PWR environment are shown in Fig. 57. The few data available for Alloys 52 and 152 are also included in the figure. Nearly 90% of the CGR data may be bounded by a curve that is a factor of eight greater than the growth rates predicted for Alloy 600 in air under the same loading conditions.

The ANL data on cyclic crack growth rates are shown in Fig. 58. They are consistent with the literature data as they also seem to show little or no environmental enhancement. Nevertheless, as with the data from the literature, Eq. 11 appears to be a good descriptor of the observed behavior. However, it also appears that most of the CGR data may be bounded by a curve that is a factor of ten greater than the growth rates predicted for Alloy 600 in air under the same loading conditions.

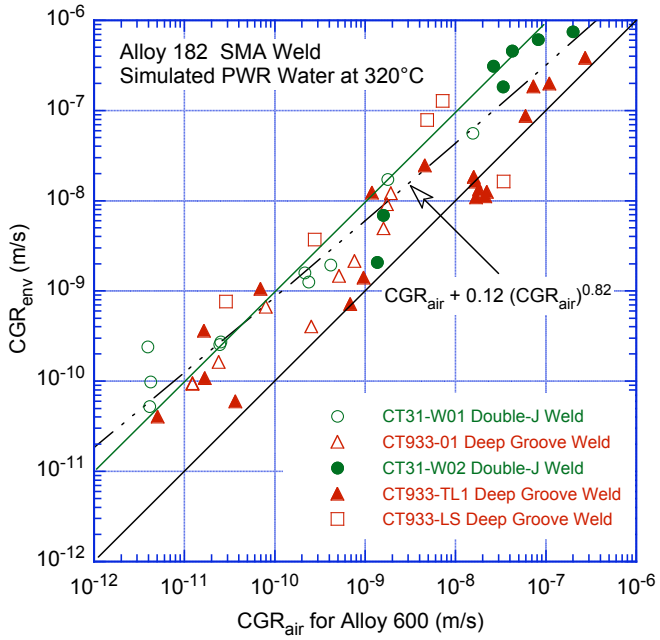

Figure 58.
CGR data for Alloy 182 SMA weld–metal specimen in simulated PWR environment at 320°C as a function of growth rates for Alloy 600 in air.

5.2. Crack Growth Rates under Constant Load

The effect of the stress intensity K on SCC crack growth for Ni–alloy welds in PWR environments has been represented by a modified[52] relationship between crack growth rate CGR_{env} (m/s) and stress intensity factor K (MPa $m^{1/2}$) originally developed by Scott to describe CGRs in steam generator tubing. However, unlike the CGR relationship for Alloy 600, the CGR relationship for Ni–alloy welds has no threshold value for the stress intensity factor K (in Alloy 600 the threshold is 9 MPa $m^{1/2}$),

$$CGR_{env} = A(K)^{1.6}. \quad (12)$$

The term A depends on the heat of the material and the temperature. The temperature dependence is usually assumed to follow an Arrhenius behavior:

$$A = \alpha \exp\left[-\frac{Q}{R}\left(\frac{1}{T} - \frac{1}{T_{ref}}\right)\right], \quad (13)$$

where: Q = activation energy for crack growth
= 130 kJ/mol (31.1 kcal/mol) for Ni–alloy welds
R = universal gas constant
= 8.314×10^{-3} kJ/mol·K (1.103×10^{-3} kcal/mol·°R)
T = absolute operating temperature in K (or °R)
T_{ref} = absolute reference temperature used to normalize the CGR data
= 598 K (1076.67°R)
α = 1.5×10^{-12} at 325°C.

The existing SCC CGR database on Ni–alloy welds in simulated PWR environments includes results from Westinghouse,[53,54] Studsvik,[47] Electricite de France (EdF),[55] CEA,[56] and ETH,[57] on Alloy 182; from Westinghouse[58] and Lockheed Martin[59] on Alloys 182 and 82; from Bechtel Bettis[60,61] on Alloy 82; and from Mitsubishi Heavy Industries (MHI)[62] on Alloy 132. The data have been obtained at temperatures between 289 and 360°C and K_{max} between 13 and 67 MPa $m^{1/2}$. A majority of the tests at EdF and all of the ETH tests were performed using wedge–opening–loaded (WOL) specimens with displacement control. The procedures for the EdF tests describe the need to check the loads at the completion of the test to determine the amount of relaxation that may have occurred, but the only data reported are for the stress intensity factors at the beginning of the test. Most of the tests at the other laboratories have been performed under active load control on specimens fatigue precracked in air.

The experimental CGRs obtained under constant load in the current tests are compared with available CGR data for Ni–alloy welds[47,53–59] in Fig. 59. The industry proposed disposition CGR curve, based on Eq. 12 for Alloy 182[52] in the PWR environment at 325°C is also plotted in the figure. The data were normalized to 325°C using Eq. 13 and an activation energy of 130 kJ/mol. Most of the existing data for Alloys 182 and 82 welds are between the Alloy 600 average curve and a factor of 10 above this curve.

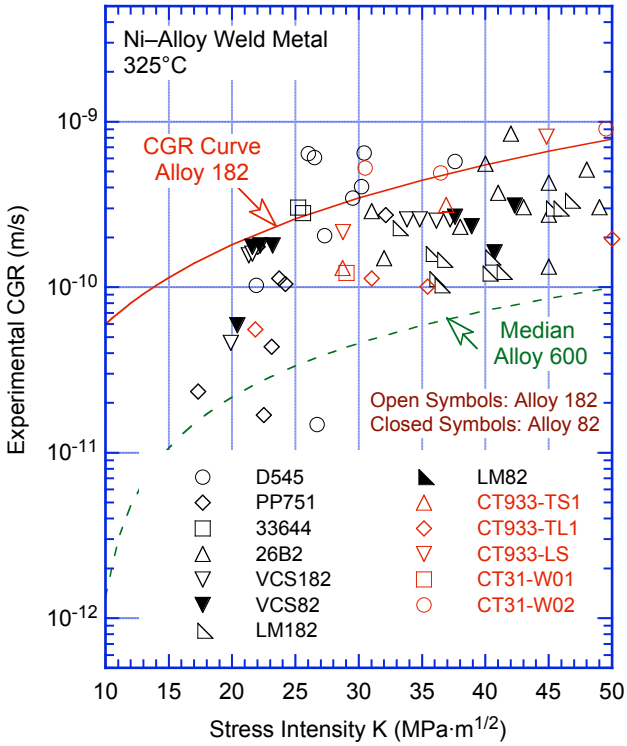

Figure 59.
Comparison of the SCC crack growth rate for the Argonne Alloy 182 weld with the available data for Alloy 182 and 82 welds in simulated PWR environment. All results normalized to 325°C using an activation energy of 130 kJ/mol. Data from Refs. 47,53–59.

Some of the earlier studies used the DC potential drop technique to estimate crack extension during the test and shed load to maintain a constant K. The presence of unbroken ligaments, time-dependent changes in the resistivity of Ni–alloys exposed to a PWR environment, and shifts in Ni/NiO stability regime with changes in dissolved hydrogen level, can result in significant uncertainties in crack length measurements. Many laboratories concluded that DC potential drop measurements of crack length were not reliable for Alloy 182,[56,61] and recommendations were made to use potential drop only to detect initiation of active crack growth and to adhere to a "one set of conditions, one test specimen" protocol so that fractographic measurements could be used to determine the change in crack length. However, in some recent studies, including the present study, the reversed current DC potential drop technique has been successfully used to monitor crack extension in Ni alloys in PWR environments.[47,58,62] The success may depend on the uniformity of the crack front. In addition, an internal reference sample made of the same material as the test specimen is commonly used to normalize the test results to compensate for possible changes in temperature, material resistivity, etc.

5.3. Effect of Key Parameters on SCC Crack Growth Rates

5.3.1 Effect of Orientation of Dendrites

Alloy 182 has a highly anisotropic structure. As the weld is deposited, dendrites grow transverse to the weld direction. Crack growth rates have been measured along the plane of the columnar grains/dendrites in a direction parallel to the columnar grains (designated TS orientation) and perpendicular to the columnar grains (designated TL orientation). Investigators at EdF concluded that although there is significant scatter, as evident in Fig. 60, the growth rates parallel to the dendrites are in general a factor 2 to 5 higher than the growth rates perpendicular to the dendrites. Similar behavior has also been observed in other studies, as shown in Fig 61. In interpreting the results in Fig. 61, note that the results for TS and LS orientations should be comparable. The crack plane for both orientations is along the columnar dendrites, although it is parallel to the direction of the weld deposit in the TS orientation and perpendicular to the direction of the weld deposit in the LS orientation. There is significant overlap in the experimental CGRs in the TL and TS orientations, e.g., the growth rates for Bechtel Bettis Alloy 82 weld C appear to be higher for the TL than TS orientation. Also, in the present study, the transition from a TG mode to IG SCC occurred sooner for the grains with dendrites perpendicular rather than parallel to the direction of crack growth.

Figure 62 shows CGR data obtained at ANL under constant load for laboratory-prepared weld alloys. Consistent with the other data in the literature,[53,54,60,61] at high K values the CGRs for cracks propagating across the direction of dendrites (orientation TL) are about a factor of two smaller than the CGRs for crack propagation along the direction of dendrites (orientations TS and LS).

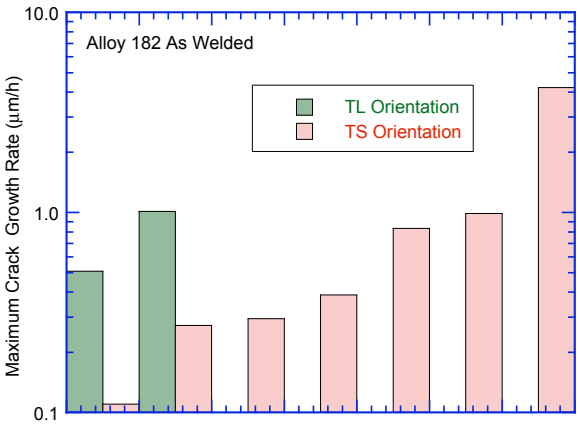

Figure 60.
Experimental crack growth rates in Alloy 182 weld in TL and TS orientations. Data from Ref. 55.

5.3.2 Effect of Size of the Experimental Crack Advance

As discussed in Section 4.2, both grain boundary type and grain orientation have an important effect on crack growth. Both Alloys 600 and 182 were found to contain increased proportions of HAB or

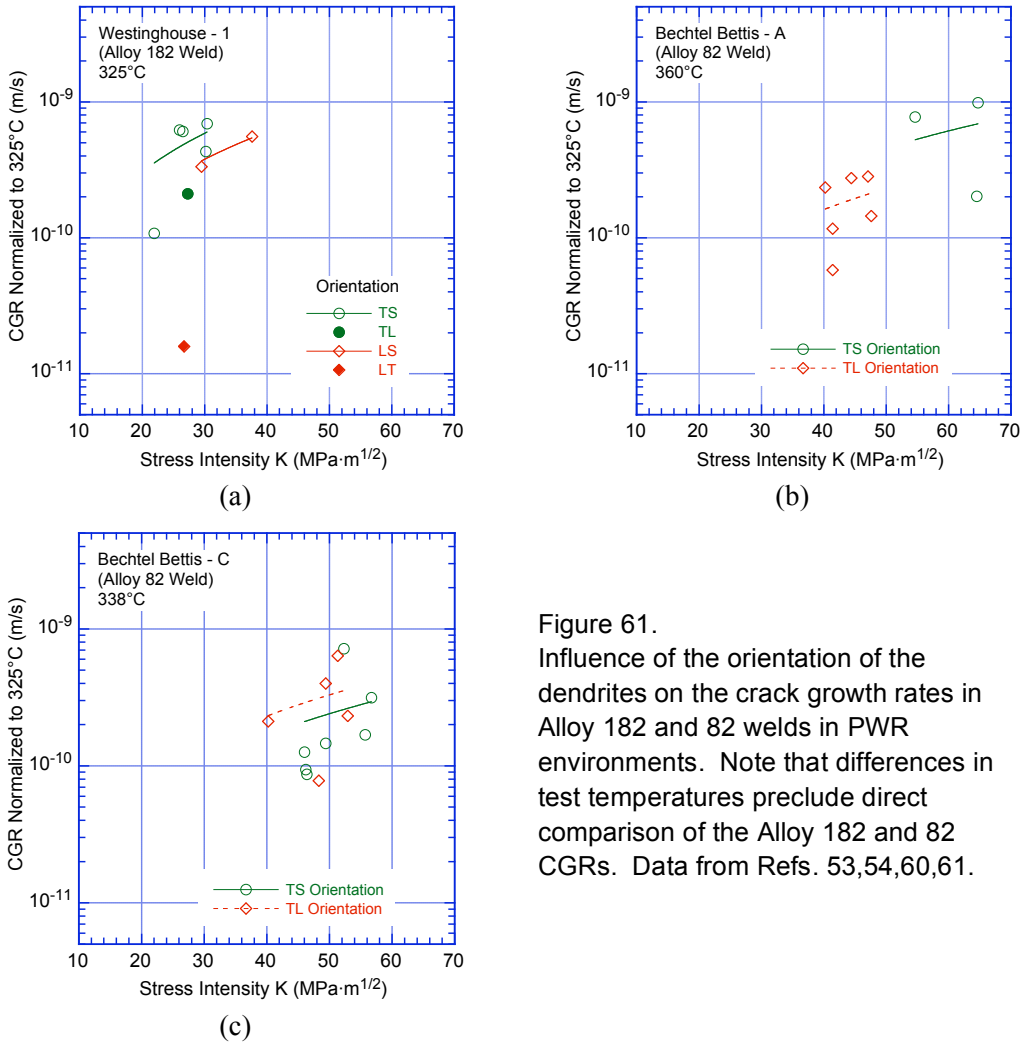

Figure 61.
Influence of the orientation of the dendrites on the crack growth rates in Alloy 182 and 82 welds in PWR environments. Note that differences in test temperatures preclude direct comparison of the Alloy 182 and 82 CGRs. Data from Refs. 53,54,60,61.

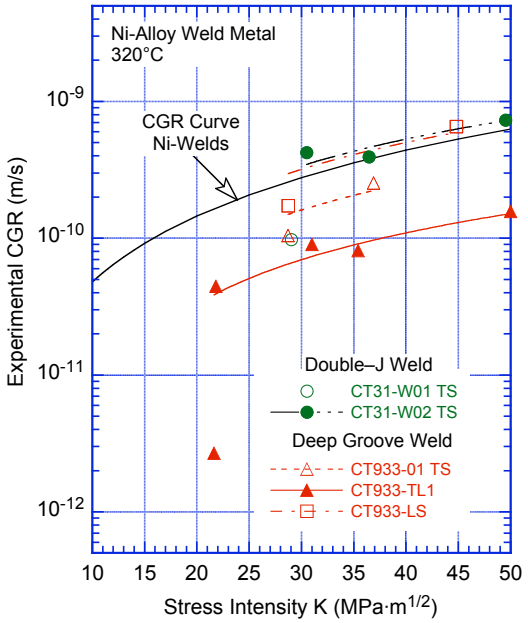

Figure 62.
SCC crack growth data for the Argonne Alloy 182 weld specimens tested.

random boundaries (≈60% in Alloy 600, and ≈70% for weld Alloy 182), well above the percolation threshold for a 2-D plane in a 3-D lattice (≈22%),[63] as would be the case of a propagating SCC crack in an alloy. Therefore, one can safely assume for simplicity that only the random boundaries participate in the cracking process, and thus, it is the uncertainty in the fraction of random boundaries that it is most likely to affect the observed crack growth. Hence, in a CGR test, the crack advance must encompass a sufficient number of grain boundaries so that the resulting CGR is representative for the alloy being investigated.

The uncertainty in the fraction of random boundaries has two sources. The first is of statistical nature and depends on the number of boundaries based on which the fraction of random boundaries is calculated. The second is of physical nature, and reflects the fact that the grain boundary character distribution is inhomogenous for any metallic material. For this analysis, we estimated the potential difference between the fraction of the cracking-susceptible HAB boundaries cracked during a test and the average number of susceptible boundaries in the material. We assumed that: (a) only HABs cracked, and (b) the HABs are distributed homogeneously in the alloy. These assumptions provide a conservative estimate for the number of grain boundaries that must be sampled.

In Alloy 600, the grain size of the material varies from 30 to 100 µm, with an average size of ≈50 µm. As shown in Table 11, a crack advance of ≈50 µm would encounter ≈440 grains across the net thickness of ≈22 mm for a 25.4–mm thick 1–T CT specimen. A simple statistical formalism by Alexandreanu and Was[45] can be used to evaluate how representative is this sample for the material being investigated. Assuming, as previously stated, that only random boundaries are susceptible to cracking and that the random boundary fraction is 60% in Alloy 600, the deviation in the fraction of susceptible random boundaries that would result from a sample of 440 grains from that typical of the material is 3.9%. Increasing the crack advance to 500 µm would reduce the deviation to 1.2%. However, the inhomogeneity in the fraction of HAB boundaries is about 12%. Thus, increasing the crack extension to 500 µm to obtain an error of 1.2%, in reality, provides no assurance that the number of boundaries tested is representative of the alloy of interest.

Table 11. Fractional errors in the population of cracking susceptible HABs as a function of alloy, orientation, and crack advance.

Alloy	Sample width, mm	Grain size,[a] mm	No. Grains along width	Crack advance, mm	No. Grains along crack	Total No. grains tested, N	Fraction HAB	Error, %
Alloy 600	22	0.05	440	0.05	1	440	0.6	3.9
	22	0.05	440	0.5	10	4400	0.6	1.2
Alloy 182 weld	22	0.05	440	0.05	1	440	0.70	3.1
TS, LS	22	0.05	440	0.5	10	4400	0.70	1.0
Alloy 182 weld	22	0.15	147	0.05	1	147	0.70	5.4
TL	22	0.15	147	0.5	3	489	0.70	3.0

[a]The grain size is as seen by the crack front.

A similar analysis can be made for Alloy 182 weld, the results are also given in Table 11. Although increasing the crack advance from 50 to 500 μm would decrease the deviation of the fraction of HABs from that representative of the material, it is not clear whether the reduction would be significant in terms of the inhomogeneity of the alloy. Although the inhomogeneity of the HAB distribution in the weld alloy has not been analyzed in detail for weld Alloy 182, the results obtained from the three OIM scans presented in a Section 4.2 suggest that the inhomogeneity in the HAB fraction in the weld materials is about 5.5%. Thus, the 5.4% difference in the fraction of HABs associated with a 50–μm crack advance in a TL-oriented specimen in a homogeneous material, shown in Table 11, is comparable to the actual inhomogeneity of the weld. As with Alloy 600, increasing the crack length to 500 μm to obtain an error of 3.0% provides little additional assurance that the material encountered is representative of the alloy tested.

5.3.3 Effect of Gentle Cycling and Periodic Unloading

Preferential growth along favorably oriented grains can lead to extremely uneven crack fronts. Even when crack advance is uniform, unbroken ligaments can be left behind the advancing crack. The ratio of maximum to average crack extension is often used to quantify the extent of engagement with the precrack.[61] Typically crack fronts become more even for larger amounts of growth. For average crack extensions less than 1 mm, the maximum crack extension is typically 2 to 4 times greater. For average crack extensions greater than 3 mm, the ratio of maximum–to–average extension is 1.3.

In recent studies a partial unload/reload cycle is often introduced during SCC crack growth tests. This test condition tends to result in a more uniform crack front and more consistent growth rates than obtained from pure constant load (or constant displacement) tests.[61] Also, specimens are often fatigue precracked in the water environment, and to assist the transition from a TG fatigue crack to IG SCC, the final precrack is performed with gentle cycling at $R \geq 0.5$ and rise times ≥1000 s. A comparison of experimental CGRs obtained with and without periodic partial unloading is shown in Fig. 63. The results obtained at different temperatures were normalized to 325°C using the Arrhenius equation and an activation energy of 130 kJ/mol. Crack growth rates obtained with unloading period ≥1000 s appear to show good agreement with the data obtained with constant load.

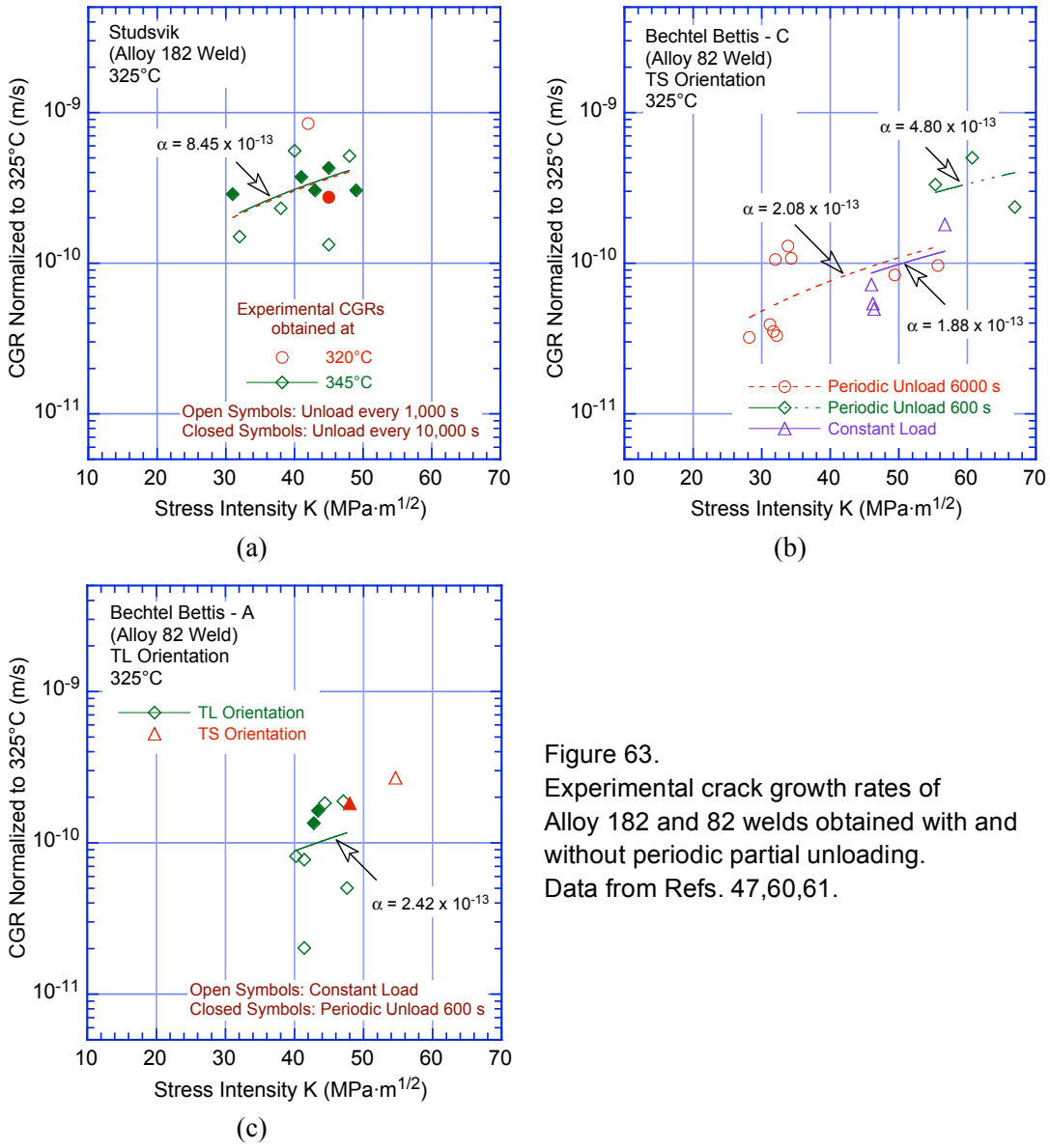

Figure 63.
Experimental crack growth rates of Alloy 182 and 82 welds obtained with and without periodic partial unloading.
Data from Refs. 47,60,61.

5.3.4 Effect of Water Chemistry

The water chemistries used for the CGR tests at Westinghouse,[53,54] Studsvik,[47] EdF,[55] and CEA[56] on Alloy 182 are fairly similar, e.g., 1000–1200 ppm B, ≈2 ppm Li, and 20–35 cc/kg dissolved hydrogen, and are characteristic of the start of the fuel cycle. Tests by Tsutsumi et al.[62] and Jacko et al.[58] were performed in PWR water with 1800 ppm B, 3.5 ppm Li, and ≈30 cc/kg dissolved hydrogen. The water chemistries for the tests at Lockheed Martin[59] used hydrogen levels of 20–40 cc/kg, and the tests at Bechtel Bettis[61] used 150 cc/kg for the tests at 360°C and 40–60 cc/kg for the tests at lower temperatures.

The effect of dissolved hydrogen level on CGRs in Ni alloys has been investigated by Morton et al. in SCC studies.[64] Several conclusions wee reached. A change in hydrogen level alters the electrochemical potential, and the growth rate exhibits a maximum at potentials in proximity to the Ni/NiO phase transition. The dependency of growth rates on dissolved hydrogen level is best described in terms of the potential relative to the Ni/NiO phase transition and not the dissolved hydrogen level. The

peak CGR at different temperatures corresponds to the potential for the Ni/NiO phase transition, which occurs at different hydrogen concentrations for different temperatures. The CGRs decrease as the electrochemical corrosion potential deviates from the corrosion potential of the Ni/NiO phase transition.

Earlier studies on primary water SCC in steam generator tubing showed relatively little dependence on variations in primary water chemistry within the current PWR water chemistry guidelines.[65] Some limited studies on Alloy 600 nozzle materials* show similar results. In most of these tests, the chemistry variables are changed one at a time, i.e., one variable is varied over the range of interest while the other variables are held at their nominal value. In the work reported in Ref. 65, a much larger effect of water chemistry was observed when several variables were changed simultaneously. However, in these tests KOH was used to vary pH so that the water chemistries were not truly prototypical of PWR primary chemistry. The effect of water chemistry on CGRs appears to be an area that requires additional study.

5.3.5 Effect of Temperature

Alloys 600 and 182 show a significant variation of CGR with temperature. For Alloy 600, activation energies for crack growth have been estimated as 130 kJ/mol (31.1 kcal/mol).[28] For Alloys 182 and 82 welds, the data sets with the most data on temperature variations are plotted in Figs. 64 as a function of 1000/T, where T is the absolute temperature in Kelvin. In Fig. 64c because the 288°C data were obtained with a 600–s unload/reload cycle, which is shown in Section 5.3.3 to result in a factor of ≈2 increase in CGRs, the data were decreased by a factor of 2. The different data sets yield activation energies that are either comparable to that observed for Alloy 600, e.g., the Bechtel Bettis[60,61] and ETH[57] data sets, or a factor of ≈2 higher, e.g., the Westinghouse,[53,54] Lockheed Martin,[59] and CEA[56] data sets. The Bechtel Bettis tests were conducted within the Ni regime, i.e., above the hydrogen concentrations for the Ni/NiO phase transition. However, the 360°C tests at 150 cc/kg hydrogen were farther removed from the Ni/NiO phase transition than the 338°C tests conducted at 40–60 cc/kg hydrogen. As discussed above in Section 5.3.4, the CGRs are highest near the Ni/NiO phase transition and decrease as the potential deviates from the Ni/NiO potential. It is possible that the CGRs in the 360°C tests may have been reduced because of the high dissolved hydrogen levels. Thus, the activation energy for the Bechtel Bettis data may be slightly higher than that determined in Fig. 64c.

Although the measured activation energies have substantial uncertainy, it appears not unreasonable to adjust data when necessary using an activation energy of 130 kJ/mol. The data suggest the possibility that the activation energy for Alloys 182 and 82 welds may be slightly higher than that for Alloy 600.

*"Crack Growth and Microstructural Characterization of Alloy 600 PWR Vessel Head Penetration Materials," Licensed Document, Electric Power Research Institute, Palo Alto, 1997.

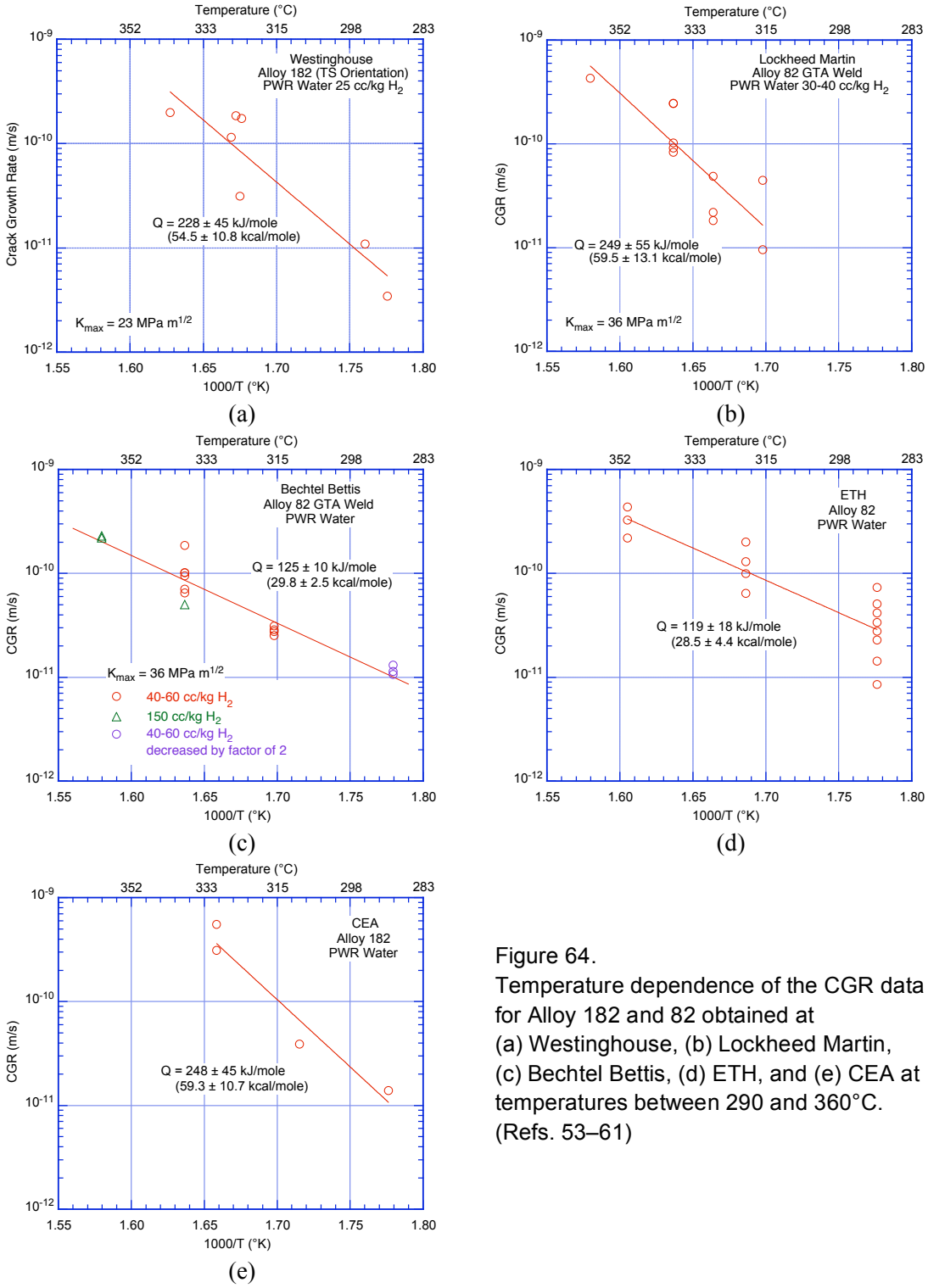

Figure 64.
Temperature dependence of the CGR data for Alloy 182 and 82 obtained at (a) Westinghouse, (b) Lockheed Martin, (c) Bechtel Bettis, (d) ETH, and (e) CEA at temperatures between 290 and 360°C. (Refs. 53–61)

5.3.6 Heat–to–Heat Comparisons of the CGR Data

The CGR vs. K plots of some of the available CGR data sets for Alloys 182 and 82 are shown in Fig. 65. To allow for incomplete initiation of SCC across the crack front the reported CGR were modified by dividing by the engagement fraction.[52] Also, the experimental CGRs were normalized to

325°C using Eq. 13, and then the best–fit parameter "α" was determined for each data set. The values of the parameter α range from 1.5 x 10^{-11} to 9.0x 10^{-10} for Alloy 182, and 5.0 x 10^{-12} to 3.5 x 10^{-10} for Alloy 82. Thus, the CGRs of Alloy 182 are typically a factor of 2.5 higher than of Alloy 82.

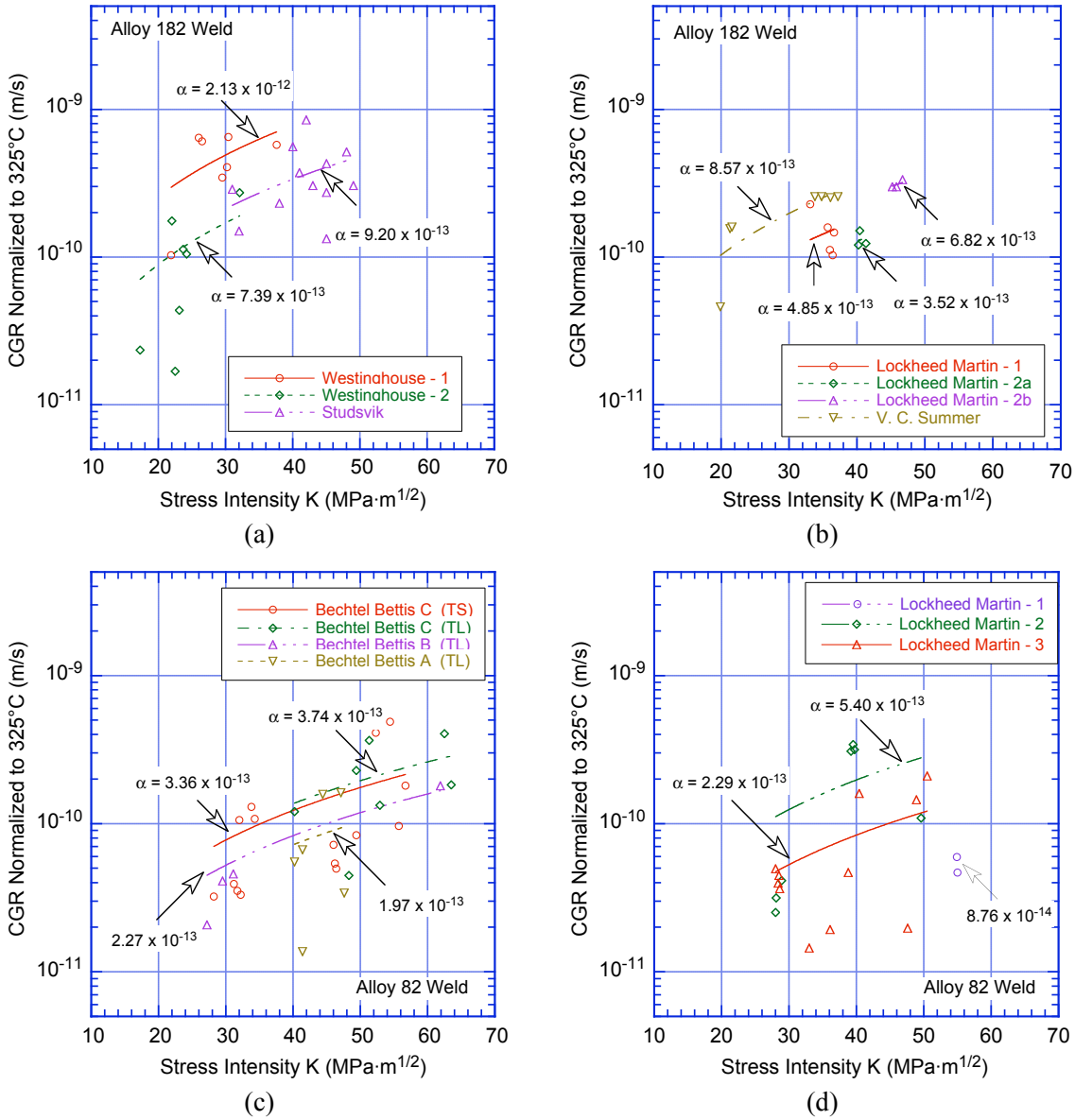

Figure 65. Experimental crack growth rate normalized to 325°C as a function of stress intensity factor K

5.3.7 Extrapolation of Available Data to the Population of Alloy 182 and 82 Weld Materials

In the selection of a disposition curve, one must consider not only how well it describes the available test data, but how it is related to the CGRs that could occur in the much larger number of heats of material that are found in the field. To do this, the values of parameter α determined from the tests on the various welds were considered as a sample from a much larger population of heats of material of interest. The values were ordered and median ranks[66,67] were used to estimate the cumulative distribution of parameter α for the population. This distribution can be fit reasonably well by a lognormal distribution. However, the experimental CGRs were first adjusted for incomplete initiation of SCC,

temperature, orientation, and alloy type, as follows: (a) divide by the engagement fraction to allow for incomplete initiation, (b) use Eq. 13 and an activation energy of 130 kJ/mole to normalize the CGRs to common reference temperature of 325°C, (c) multiply CGRs for TL orientations by 2 to account for orientation effects, and (d) multiply CGRs for Alloy 82 welds by 2.5 to account for the effects of alloy type. Also, studies at CEA[56] generally report only the maximum values of CGR; the average CGRs were determined from the maximum values using the correlation proposed by Attanasio et al.[59] The ratio between the maximum and average CGR was assumed to be the same as the ratio between maximum and average crack extension, i.e., $R = \Delta a_{max}/\Delta a_{ave}$. The ratio R is expressed as

$$\ln(R - 1) = 2.48 - 0.762 \ln(\Delta a_{ave}/0.051), \quad (14)$$

where crack extension is in mm. The normalized CGR data for the various Ni-alloy welds are presented in Table 12. The distributions for (a) the data that satisfy the screening criterion of Ref. 52 and (b) all the existing data are plotted with a log scale for α in Figs. 66a and b, respectively. The values of log mean and log standard deviation for the screened data and all the data are –27.795 and 0.650, and –27.768 and 0.563, respectively. Thus the median and 75th percentile values of parameter α are 8.55×10^{-13} and 1.32×10^{-12} and, 8.72×10^{-13} and 1.27×10^{-12}, respectively. The difference between the analyses with the screened data and all the data is insignificant. The estimated uncertainties for various data sets are also shown in the figure. The value of α that describes the 75th percentile of this distribution would give a CGR model that would be expected to bound the CGRs of 75% of the heats of Alloy 182 welds in the population.

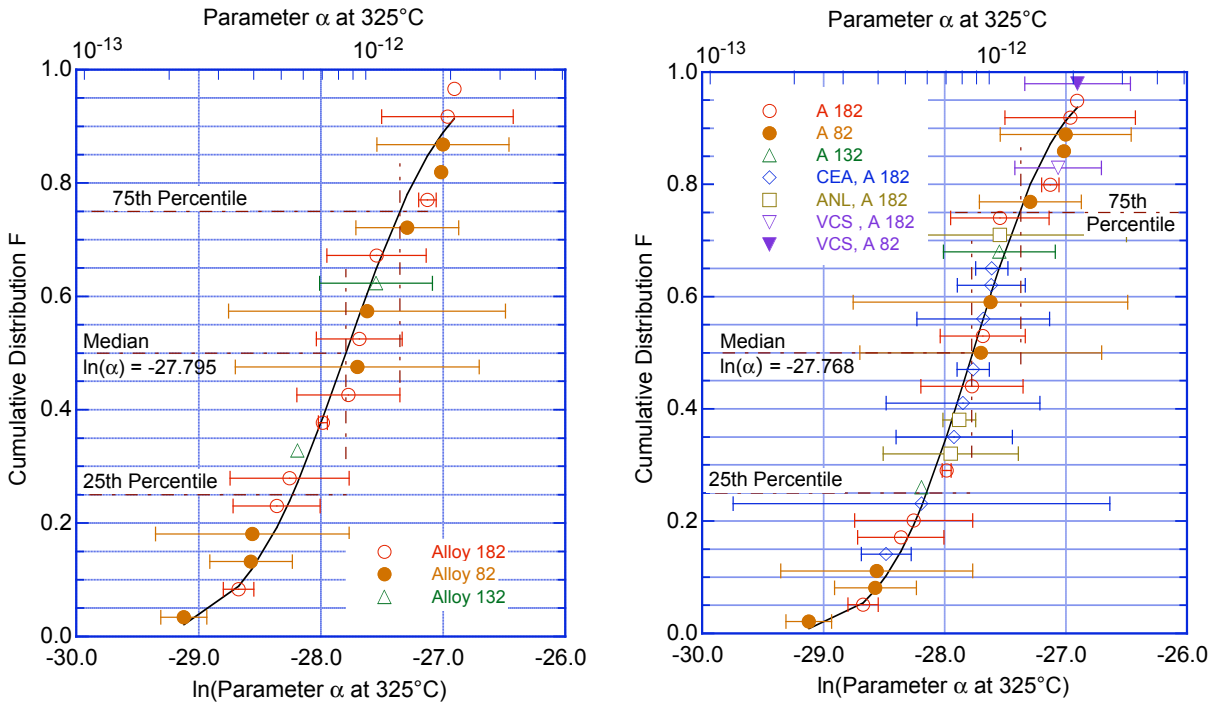

Figure 66. Estimated cumulative distribution of the normalized parameter α in the CGR relationship for Alloy 182 based on (a) data that satisfy the screening criterion of Ref. 52 and (b) all the data.

Table 12. Values of the parameter A in the Scott model for crack growth rate [Eq. (12)] for several Alloy 182, 82, and 132 welds.

Heat No.	Alloy	Orientation	Ln(Parameter α)	Std Deviation	Data Points	Reference
WH 182 - 1*	A 182	TS	-25.964	0.538	7	53,54
WH 182 - 1*	A 182	TL	-26.908	–	1	46,47
WH 182 - 2*	A 182	TS	-27.685	0.351	3	53,54
WH 182 - 3*	A 182	TS	-27.128	0.072	2	53,54
Studsvik 26B2*	A 182	TS	-27.544	0.405	5	12,47
Studsvik 6892*	A 182	TS	-27.775	0.422	2	12,47
Studsvik WC05F8*	A 182	TS	-28.256	0.486	8	12,47
LM 182 - 1*	A 182	TS	-28.361	0.357	5	59
LM 182 - 2a*	A 182	TS	-28.673	0.124	3	59
LM 182 - 2b*	A 182	TS	-27.983	0.036	3	59
LM 82 - 2*	A 82	TS	-27.701	0.997	6	59
LM 82 - 3*	A 82	TS	-28.559	0.792	11	59
LM 82 - 1*	A 82	TS	-29.121	0.188	2	59
A-1*	A 82	TL	-27.294	0.420	3	61
C-1*	A 82	TL	-27.002	0.540	3	61
C-2*	A 82	TL	-27.623	1.133	2	61
C-3*	A 82	TS	-27.016	–	1	61
C-4*	A 82	TS	-28.571	0.338	6	61
MHI MG7*	A 132	TS/LS	-27.548	0.462	3	62
MHI 132*	A 132	LS	-28.191	–	1	62
CEA 182 D545	A 182	TL	-28.191	1.555	4	56
CEA 182 M1	A 182	TL	-27.848	0.634	2	56
CEA 182 M2	A 182	TL	-27.765	0.132	2	56
CEA 182 M4	A 182	TL	-27.611	0.133	2	56
CEA 182 D545 SR	A 182	TL	-27.614	0.280	2	56
CEA 182 M1 SR	A 182	TL	-28.482	0.205	2	56
CEA 182 M2 SR	A 182	TL	-27.921	0.480	2	56
CEA 182 M4 SR	A 182	TL	-27.682	0.547	2	56
VCS Weld	A 82	TS	-26.903	0.436	8	58
VCS Butter	A 182	TL	-27.062	0.356	8	58
ANL Double J*	A 182	TS	-27.545	1.045	4	This study
ANL Deep Groove*	A 182	TS	-27.948	0.558	5	This study
ANL Deep Groove*	A 182	TL	-27.878	0.135	4	This study

*Dataset satisfy the screening criterion of Ref. 52.

Two sources of error are possible in the distribution in Fig. 66. One is the difficulty of determining the parameters of the full lognormal distribution from only a few samples. We have determined a sample mean and sample standard deviation. We need the population mean and population standard deviation.[68] Confidence bounds can be obtained on the population mean and standard deviation in terms of the sample mean and standard deviation. Even this, however, does not fully address the uncertainty in the distribution, because of the large uncertainties in the sample values themselves, i.e., the "horizontal" uncertainty in the actual value of parameter α, as indicated by the error bars in Fig. 66.

To assess the effect of these uncertainties on the population statistics, we performed a Monte Carlo analysis, in which a series of distributions was generated by sampling from the distributions for the value of α for each heat defined by the uncertainty for the particular heat. Each of these distributions was then used to estimate the mean value and standard deviation of the lognormal distribution for the population. Because the log of the mean and the log of the standard deviation of α are distributed normally, in the following discussion, the term "mean" and "standard deviation" will be used as shorthand for "log mean" and "log standard deviation", and the discussion will focus on properties of normal distributions. The sample means will be denoted as α_s, the population means as α_t; the sample standard deviation is s, the population standard deviation is σ.

For a normal distribution the quantity

$$\frac{(n-1)s^2}{\sigma^2}, \tag{15}$$

where n is the number of samples, has a χ^2 distribution with n – 1 degrees of freedom.[68] The quantity

$$\frac{\alpha_s - \alpha_t}{s}\sqrt{n} \tag{16}$$

has a t distribution with n – 1 degrees of freedom.[68] For each sample mean and standard deviation generated by the Monte Carlo analysis, an estimate of the population standard deviation and mean were obtained by sampling from the χ^2 and t distributions and using Eqs. 15 and 16. Values of the 95th, 90th, 75th, and 50th percentile values for each of the population distributions were calculated. Five–thousand Monte Carlo cases were run to develop distributions for 95th, 90th, 75th, and 50th percentile values. The results of the Monte Carlo analysis are summarized in Table 13 in terms of α values that bound the portion of the population we wish to consider and the confidence that we wish to have in the estimates of the bounds. With small sample sizes, demanding too high a confidence level can lead to very conservative estimates of the percentile values.

Table 13. Values of the parameter α for Alloy 182 and 82 at 325°C as a function of the percentage of the population bounded and the confidence level.

Confidence	Population Percentage			
Level	95	90	75	50
50	2.47×10^{-12}	1.95×10^{-12}	**1.32×10^{-12}**	8.55×10^{-13}
75	3.41×10^{-12}	2.68×10^{-12}	1.78×10^{-12}	1.14×10^{-12}
90	4.99×10^{-12}	3.84×10^{-12}	2.48×10^{-12}	1.53×10^{-12}
95	5.93×10^{-12}	4.53×10^{-12}	2.88×10^{-12}	1.74×10^{-12}

Cumulative distributions for these values can be obtained by rank ordering the values and then approximating the cumulative distribution by median ranks.[66] These distributions are shown in Fig. 67. By considering, for example, the distribution for the 95th percentile values, one can determine the value at the desired confidence bounds corresponding to F= 0.5, 0.75, 0.9, and 0.95. Order statistics[69] can be used to show that with 5000 values, the confidence bounds on the percentile values determined from these distributions are quite narrow. The 75th percentile value of α at a 50% confidence level is 1.32×10^{-12}.

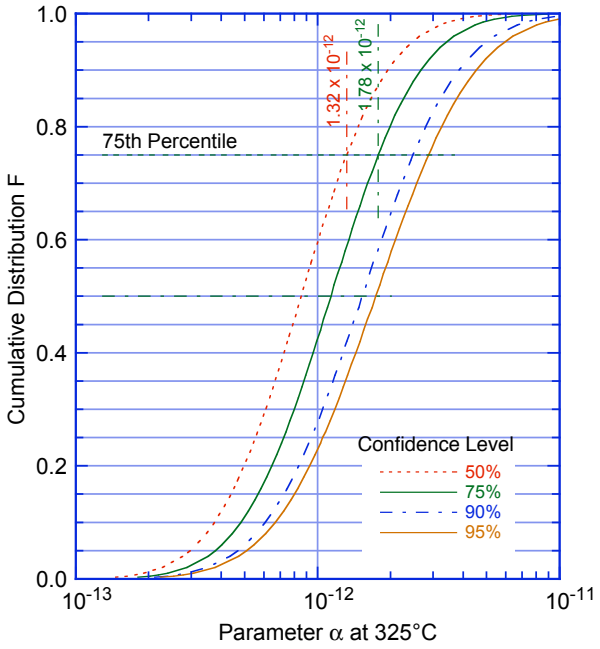

Figure 67.
Distributions of the 95th, 90th, 75th, and 50th confidence levels for parameter α for heats of Alloy 182 welds in PWR water at 325°C.

This is a "best estimate" (50% confidence level) that it bounds 75% of the population. This curve is compared with the experimental CGR data for Alloy 182 (including ANL data) and Alloy 82 in Fig. 68a and b, respectively.

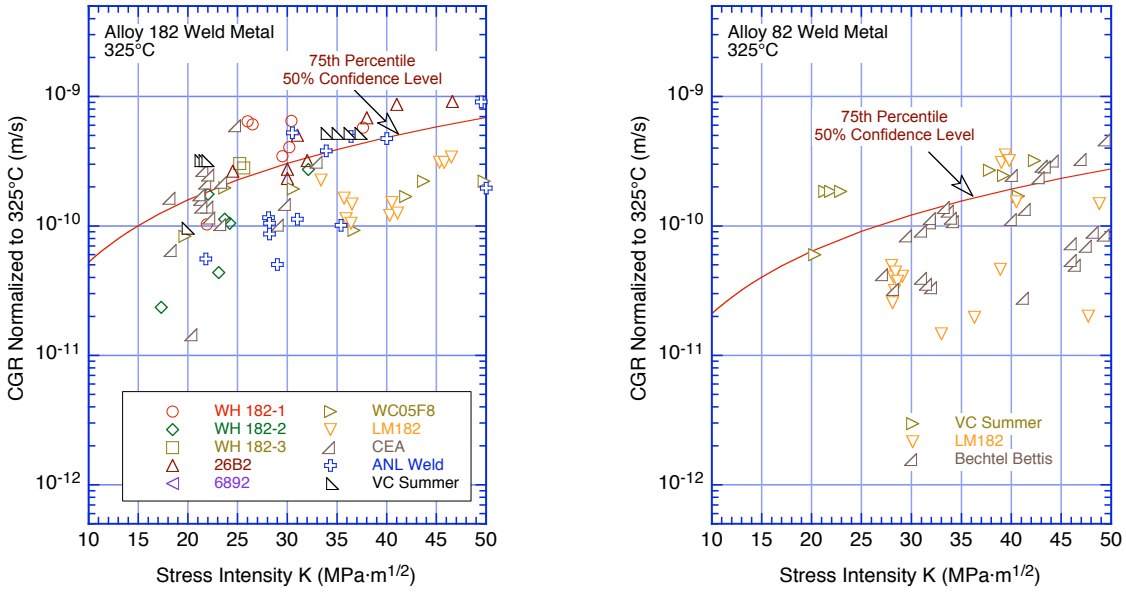

(a) (b)

Figure 68. Comparison of the SCC crack growth rate for (a) Alloy 182 and (b) Alloy 82 welds in simulated PWR environment with the 75th percentile curve.

6 Summary

Crack growth rate results are presented for Alloy 182 shielded metal arc (SMA) weld metal in the simulated PWR environment at 320°C. The weld had either a double "J" joint or a deep-groove design.

Metallographic examinations were performed to characterize the microstructure of the weld. The weld structure consisted of vertically columnar grains and dendrites. The weld microstructure was also examined by orientation imaging microscopy to determine the orientations of the grains and the type of grain boundaries present. The results indicate that the intragranular dendrites are coherent and are, therefore, expected to be very resistant to cracking. The proportion of cracking–resistant coincident–site lattice boundaries in the weld was found to be relatively small (≈30%) by comparison with that of Alloy 600 in a solution-annealed condition (≈50%). The comparison suggests that Alloy 182 is more susceptible to cracking than Alloy 600, and this inference is supported by the findings presented in this report. However, the same OIM maps have revealed the clustering of grains with similar orientation in the weld alloy. In addition, an OIM analysis along the crack path in the weld specimens found that boundaries separating grains of similar orientation are more resistant to cracking than boundaries separating grains of different orientations. That is, the clustering of grains with similar orientations in weld alloys resulted in a different class of random boundaries that are more resistant to SCC. As such, it appears that grain orientation emerges as a SCC-determining parameter that should be included along with grain boundary misorientation for a better description of a weld alloy's susceptibility to SCC. A first necessary step would include a precise quantification of the prevalence of this class of boundaries in weld alloys.

Crack growth tests were conducted on 25.4-mm thick 1–T compact tension specimens with different orientations relative to the weld columnar grains. Crack extensions were monitored by the reversing DC potential difference method. The final crack extension estimated from the DC potential method was verified by physical measurements on the fracture surfaces.

The environmental enhancement of CGRs under cyclic loading was determined relative to the CGRs that would be expected under the same loading conditions for Alloy 600 in air. The results indicate little or no environmental enhancement of CGRs for Alloy 182 weld metal in the PWR environment. The CGRs of Alloy 182 in the PWR environment are a factor of ≈5 higher than those of Alloy 600 in air under the same loading conditions.

The experimental CGR for the Alloy 182 weld obtained under essentially a constant load with periodic partial unloading is close to that expected for the median behavior of Alloy 600 in the PWR environment. Most of the existing CGR data for Alloy 182 and 82 welds are a factor of 1-10 greater than the median value for Alloy 600.

Metallographic examination of the fracture surface revealed a relatively straight crack front. The fracture mode correlated well with the test condition. Specifically, it was found that high rise times or long hold periods favor IG SCC. Also, IG cracking apparently advanced more readily along some grain orientations than others, resulting in a crack front with occasional unbroken ligaments and few regions of TG cracking.

The existing CGR data for Ni–alloy weld metals have been compiled and evaluated to establish the effects of key material, loading, and environmental parameters on CGRs in PWR environments. The

results from the present study were compared with the existing CGR data to determine the relative susceptibility of the specific Ni–alloy weld to SCC and corrosion fatigue.

The limited data in the literature and results from the present study indicate very little frequency–dependent environmental enhancement of fatigue CGRs of Alloy 182 and 82 welds in PWR environments. Under the same loading conditions, strain–rate–dependent environmental enhancement is observed in Alloy 600.

The SCC CGRs of Ni–alloy welds are influenced by several material and environmental parameters. In general, the CGRs are higher for Alloy 182 than Alloy 82. Although there is significant scatter in the results, the CGRs along the plane of the columnar grains are higher in a direction parallel than perpendicular to the columnar grains. The existing data suggest that the activation energy for the temperature dependence of SCC CGRs for Alloy 182 and 82 weld metals may be slightly higher than that for Alloy 600. Individual data sets yield activation energies between 120–250 kJ/mol (28.5–59.5 kcal/mol). Studies on the effect of dissolved hydrogen on SCC CGRs in Alloy 182 and 82 welds indicate a maximum in proximity to the electrochemical potential of the Ni/NiO phase transition. The CGRs decrease as the electrochemical corrosion potential deviates from the corrosion potential of the Ni/NiO phase transition.

The effect of the stress intensity factor K on SCC crack growth for Ni–alloy welds is represented by the Scott model. Heat–to–heat comparisons of the CGR data were made. The cumulative distribution of the parameter A in the Scott model was used to estimate the heat–to–heat variability of the population of Alloy 182 and 82 welds. Values of the parameter A as a function of the percentage of the population bounded and the confidence level were determined. Under similar loading and environmental (PWR) conditions, the mean CGRs for Ni–alloy welds appear to be a factor of ≈2 higher than the mean CGRs for Alloy 600.

References

1. Scott, P., "An Analysis of Primary Water Stress Corrosion Cracking in PWR Steam Generators," Proc. of the Specialists Meeting on Operating Experience with Steam Generators, Brussels, Belgium, pp. 5–6, 1991.

2. Cattant, F., "Lessons Learnt from the Examination of Tubes Pulled from Electricite de France Steam Generators," Nucl. Eng. Des. 168, pp. 241–253, 1997.

3. Diercks, D. R., W. J. Shack, and J. Muscara, "Overview of Steam Generator Tube Degradation and Integrity Issues," Nucl. Eng. Des. 194, pp. 19–30, 1999.

4. USNRC Information Notice No. 90–10, "Primary Water Stress Corrosion Cracking (PWSCC) of Inconel 600," Feb. 1990.

5. USNRC Generic Letter 97-01, "Degradation of Control Rod Drive Mechanism and Other Vessel Closure Head Penetrations," April 1, 1997.

6. Economou, J., A. Assice, F. Cattant, J. Salin, and M. Stindel, "NDE and Metallurgical Examination of Vessel Head Penetrations," 3rd Intl. Symp. of Fontevraud, Sept. 12–16, 1994.

7. Robinson, M. R., Duke Power Company, "Oconee Unit 1 and Unit 3 Reactor Vessel Head Leakage, Cracking of RV Head Penetrations due to Primary Water Stress Corrosion Cracking," NRC Meeting with the NEI EPRI Material Reliability Program Regarding CRDM Nozzle Crackling Issues, Rockville, MD, April 12, 2001.

8. Frye, C. R., T. Alley, M. L. Arey, Jr., and M. R. Robinson, "Cracking in Alloy 600/182 Reactor Vessel Head Penetrations," PVP–Vol. 437, Service Experience and Failure Assessment Applications ASME 2002, P. S. Lam, ed., American Society of Mechanical Engineers, New York, pp. 171–178, 2002.

9. USNRC Information Notice 2001–05, "Through–Wall Circumferential Cracking of Reactor Pressure Vessel Head Control Rod Driver Mechanism Penetration Nozzle at Oconee Nuclear Station, Unit 3," April 30, 2001.

10. USNRC Bulletin 2001–01, "Circumferential Cracking of Reactor Pressure Vessel Head Penetration Nozzles," Aug. 3, 2001.

11. USNRC Information Notice 2000–17, "Crack in Weld Area of Reactor Coolant System Hot Leg Piping at V. C. Summer," Oct. 18, 2000; Suppl. 1, Nov. 16, 2000; Suppl. 2, Feb. 28, 2001.

12. Jenssen, A., K. Norrgard, J. Lagerstrom, G. Embring, and D. Tice, "Assessment of Cracking in Dissimilar Metal Welds," in Proc. of the Tenth Intl. Conf. on Environmental Degradation of Materials in Nuclear Power Systems-Water Reactors, NACE International, Houston, TX, 2001.

13. Bennetch, J. I., G. E. Modzelewski, L. L. Spain, and G. V. Rao, "Root Cause Evaluation and Repair of Alloy 82/182 J–Groove Weld Cracking of Reactor Vessel Head Penetrations at North Anna Unit 2," PVP–Vol. 437, Service Experience and Failure Assessment Applications ASME 2002, P. S. Lam, ed., American Society of Mechanical Engineers, New York, pp. 179–185, 2002.

14. USNRC Information Notice 2002–11, "Recent Experience with Degradation of Reactor Pressure Vessel Head," March 12, 2002.

15. USNRC Information Notice 2003–11, "Leakage Found on Bottom–Mounted Instrumentation Nozzles," Aug. 13, 2003; Suppl. 1, Jan. 8, 2004.

16. USNRC Bulletin 2003–02, "Leakage from Reactor Pressure Vessel Lower Head Penetrations and Reactor Coolant Pressure Boundary Integrity," Aug. 21, 2003.

17. Ruther, W. E., W. K. Soppet, and T. F. Kassner, "Corrosion Fatigue of Alloys 600 and 690 in Simulated LWR Environments," NUREG/CR–6383, ANL–95/37, April 1996.

18. Ruther, W. E., W. K. Soppet, and T. F. Kassner, "Environmentally Assisted Cracking of Alloys 600 and 690 in Simulated LWR Water," Environmentally Assisted Cracking in Light Water Reactors, Semiannual Report, July 1997–December 1997, NUREG/CR–4667, Vol. 25, ANL–98/18, pp. 42–75, Sept. 1998.

19. Ruther, W. E., W. K. Soppet, T. F. Kassner, and W. J. Shack, "Environmentally Assisted Cracking of Alloys 600 and 690 in Simulated LWR Water," Environmentally Assisted Cracking in Light Water Reactors, Semiannual Report, January 1998–July 1998, NUREG/CR–4667, Vol. 26, ANL–98/18, pp. 25–32, March 1999.

20. Ruther, W. E., W. K. Soppet, T. F. Kassner, and W. J. Shack, "Environmentally Assisted Cracking of Alloys 600 and 690 in Simulated LWR Water," Environmentally Assisted Cracking in Light Water Reactors, Semiannual Report, July 1998–December 1998, NUREG/CR–4667, Vol. 27, ANL–99/11, pp. 45-54, October 1999.

21. Soppet, W. K., O. K. Chopra, and W. J. Shack, "Environmentally Assisted Cracking of Alloys 600 and 690 in Simulated LWR Water," Environmentally Assisted Cracking in Light Water Reactors, Semiannual Report, July 1999–December 1999, NUREG/CR–4667, Vol. 29, ANL–00/23, pp. 39-45, November 2000.

22. Chopra, O. K., W. K. Soppet, and W. J. Shack, "Effects of Alloy Chemistry, Cold Work, and Water Chemistry on Corrosion Fatigue and Stress Corrosion Cracking of Nickel Alloys and Welds," NUREG/CR–6721, ANL–01/07, April 2001.

23. Cassagne, T. B., and A. Gelpi, "Crack Growth Rate Measurements on Alloy 600 Steam Generator Tubes in Steam and Primary Water," Proc. of the Fifth Intl. Symp. on Environmental Degradation of Materials in Nuclear Power Systems-Water Reactors, American Nuclear Society, La Grange Park, IL, pp. 518–524, 1991.

24. Foster, J. P., W. H. Bamford, and R. S. Pathania, "Initial Results of Alloy 600 Crack Growth Rate Testing in a PWR Environment," Proc. of the Seventh Intl. Symp. on Environmental Degradation of Materials in Nuclear Power Systems-Water Reactors, NACE International, Houston, TX, pp. 25–39, 1995.

25. Magdowski, R., F. Vaillant, C. Amzallag, and M. O. Speidel, "Stress Corrosion Crack Growth Rates of Alloy 600 in Simulated PWR Coolant," Proc. of the 8th Intl. Symp. on Environmental Degradation of Materials in Nuclear Power Systems-Water Reactors, S. M. Bruemmer, ed., American Nuclear Society, La Grange Park, IL, pp. 333–338, 1997.

26. Le Hong, S., C. Amzallag, and A. Gelpi, "Modeling of Stress Corrosion Crack Initiation on Alloy 600 in Primary Water of PWRs," Proc. of the Ninth Intl. Symp. on Environmental Degradation of Materials in Nuclear Power Systems-Water Reactors, F. P. Ford, S. M. Bruemmer, and G. S. Was, eds., The Minerals, Metals, and Materials Society, Warrendale, PA, pp. 115–122, 1999.

27. Raquet, O., and G. Santarini, "Stress Corrosion Crack Propagation Rate of Alloy 600 in the Primary Water of PWR Influence of a Cold Worked Layer," Proc. of the Ninth Intl. Symp. on Environmental Degradation of Materials in Nuclear Power Systems-Water Reactors, F. P. Ford, S. M. Bruemmer, and G. S. Was, eds., The Minerals, Metals, and Materials Society, Warrendale, PA, pp. 207–213, 1999.

28. White, G. A., Hickling, J., and Mathews, L. K., "Crack Growth Rates for Evaluating PWSCC of Thick–Wall Alloy 600 Material," Proc. of the 11th Intl. Symp. on Environmental Degradation of Materials in Nuclear Power Systems-Water Reactors, NACE International, Houston, TX, pp. 166–179, 2003.

29. Macdonald, D. D., A. C. Scott, and P. Wentrcek, "External Reference Electrodes for Use in High Temperature Aqueous Systems," J. Electrochem. Soc. 126, pp. 908–911, 1979.

30. Andresen, P. L., and P. G. Campbell, "The Effects of Crack Closure in High–Temperature Water and its Role in Influencing Crack Growth Data," Proc. of the Fourth Intl. Symp. on Environmental Degradation of Materials in Nuclear Power Systems-Water Reactors, D. Cubicciotti, ed., NACE International, Houston, TX, pp. 4.86–4.111, 1990.

31. Briant, C. L., and E. L. Hall, "The Microstructural Causes of Intergranular Corrosion of Alloys 82 and 182," Corrosion, 43, pp. 539–548, 1987.

32. Palumbo, G., K. T. Aust, E.M. Lehockey, U. Erb, and P. Lin, "On a more Restrictive Geometric Criterion for 'Special' CSL Grain Boundaries," Acta Metallurgica, 14, pp. 1685-1690, 1998.

33. Was, G., V. Thaveeprungsriporn, and D. C. Crawford, "Grain Boundary Misorientation Effects on Creep and Cracking in Ni-Based Alloys," Journal of Materials, 50 (2), pp. 44-49, 1998.

34. Alexandreanu, B., B. Capell, and G. S. Was, "Combined Effect of Special Grain Boundaries and Grain Boundary Carbides on IGSCC of Ni-16Cr-9Fe-xC Alloys," Materials Science and Engineering A, 300, pp. 94-104, 2001.

35. Lehockey, E. M., G. Palumbo, and P. Lin, "Improving the Weldability and Service Performance of Nickel- and Iron-Based Superalloys by Grain Boundary Engineering," Metallurgical and Materials Transactions, 29 (12), pp. 369-379, 1998.

36. Brandon D.G., "The structure of high-angle grain boundaries", Acta Metallurgica, 14, pp 1479-1484, 1966.

37. Palumbo, G., P.J. King, and K.T. Aust, "Grain Boundary Design and Control for Intergranular Stress Corrosion Resistance," Scripta Metallugica et Materialia, 25 (8), pp. 1775-1780, 1991.

38. Cheung, C., U. Erb, and G. Palumbo, "Application of Grain Boundary Engineering Concepts to Alleviate Intergranular Cracking in Alloys 600 and 690," Materials Science and Engineering A, 185, pp. 39-43, 1994.

39. Gertsman, V. I., and S.M. Bruemmer, "Study of Grain Boundary Character along Intergranular Stress Corrosion Crack Paths in Austenitic Alloys," Acta Materialia, 49, pp. 1589–1598, 2001.

40. Pan, Y., B. L. Adams, T. Olson, and N. Panayotou, "Grain-Boundary Structure Effects on Intergranular Stress Corrosion Cracking of Alloy X-750," Acta Materialia, 44 (12), pp. 4685-4695, 1996.

41. Lehockey, E. M., A.M. Brennenstuhl, and I. Thompson, "On the Relationship between Grain Boundary Connectivity, Coincident Site Lattice Boundaries, and Intergranular Stress Corrosion Cracking," Corrosion Science, 46, pp. 2383–2404, 2004.

42. Yi, Y. S., and J. S. Kim, "Characterization Methods of Grain Boundary and Triple Junction Distributions," Scripta Materialia 50, pp. 855–859, 2004.

43. Schuh, C. A., R. W. Minich, and M. Kumar, "Connectivity and Percolation in Simulated Grain–Boundary Networks," Phil. Mag. 83 (6), pp. 711-726, Feb. 21, 2003.

44. Alexandreanu, B., and G. S. Was, "Grain Boundary Deformation–Induced Intergranular Stress Corrosion Cracking of Ni-16Cr-9Fe in 360°C Water," Corrosion 59 (8), 705, 2003.

45. Alexandreanu, B., and G. S. Was, "A Priori Determination of the Sampling Size for Grain Boundary Character Distribution and Grain Boundary Degradation Analysis," Phil. Mag. A, 81 (8), pp. 1951-1965, 2001.

46. Wright, S.I., and D.P. Field, "Recent Studies of Local Texture and its Influence on Failure," Materials Science and Engineering A, 257, pp. 165–170, 1998.

47. Lindstrom, R., P. Lidar, and J. Lagerstrom, "Crack Growth of Alloy 182 in Simulated Primary Side PWR Environment," Proc. of the 8th Intl. Symp. on Environmental Degradation of Materials in Nuclear Power Systems-Water Reactors, S. M. Bruemmer, ed., American Nuclear Society, La Grange Park, IL, pp. 422–429, 1997.

48. Amzallag, C., G. Baudry, and J. L. Bernard, "Effects of PWR Environment on the Fatigue Crack Growth of Different Stainless Steels and Inconel Type Alloy," Proc. IAEA-Specialists Meeting on Subcritical Crack Growth, NUREG/CP–0044, Vol. 1, pp. 263–294, 1983.

49. Van Der Sluys, W. A., B. A. Young, and D. Doyle, "Corrosion Fatigue Properties on Alloy 690 and some Nickel–Based Weld Metals," Assessment Methodologies for Preventing Failure: Service Experience and Environmental Considerations, PVP Vol. 410-2, R. Mohan, ed., American Society of Mechanical Engineers, New York, pp. 85–91, 2000.

50. Psaila–Dombrowski, M. J., C. S. Wade, J. M. Sarver, W. A. Van Der Sluys, and P. E. Doherty, "Evaluation of Weld Metals 82, 152, 52, and Alloy 690 Stress Corrosion Cracking and Corrosion Fatigue Susceptibility," Proc. of the 8th Intl. Symp. on Environmental Degradation of Materials in Nuclear Power Systems-Water Reactors, S. M. Bruemmer, ed., American Nuclear Society, La Grange Park, IL, pp. 412–421, 1997.

51. James, L. A., and W. J. Mills, "Fatigue–Crack Propagation Behavior of Wrought Alloy 600 and Weld–Deposited EN82H in an Elevated Temperature Aqueous Environment," Service Experience, Structural Integrity, Severe Accident, and Erosion in Nuclear and Fossil Plants, PVP Vol. 303, The American Society of Mechanical Engineers, pp. 21–36, 1995.

52. White, G., J. Hickling, and C. Harrington, "MRP Development of Crack Growth Rate Disposition Curves for Primary Water Stress Corrosion Cracking (PWSCC) of Thick-Section Alloy 600 Components and Alloy 82, 182 and 132 Weldments," 2005 EPRI International PWSCC of Alloy 600 Conference, Santa Ana Pueblo, NM, March 7-10, 2005.

53. Bamford, W. H., J. P. Foster, and R. S. Pathania, "An Investigation of Alloy 182 Stress Corrosion Cracking in Simulated PWR Environment," Proc. of the Ninth Intl. Symp. on Environmental Degradation of Materials in Nuclear Power Systems-Water Reactors, F. P. Ford, S. M. Bruemmer, and G. S. Was, eds., The Minerals, Metals, and Materials Society, Warrendale, PA, pp. 279–294, 1999.

54. Bamford, W. H., J. P. Foster, K. R. Hsu, L. Tunon–Sanur, and A. McIlree, "Alloy 182 Weld Crack Growth, and its Impact on Service–Induced Cracking in Operating PWR Plant Piping," Proc. Tenth Intl. Conf. on Environmental Degradation of Materials in Nuclear Power Systems-Water Reactors, NACE International, Houston, TX, 2001.

55. Le Hong, S., J. M. Boursier, C. Amzallag, and J. Daret, "Measurement of Stress Corrosion Cracking Growth Rates in Weld Alloy 182 in Primary Water of PWR," Proc. Tenth Intl. Conf. on Environmental Degradation of Materials in Nuclear Power Systems-Water Reactors, NACE International, Houston, TX, 2001.

56. Cassagne, T., D. Caron, J. Daret, and Y. Lefevre, "Stress Corrosion Crack Growth Rate Measurements in Alloys 600 and 182 in Primary Loops Under Constant Load," Proc. of the Ninth Intl. Symp. on Environmental Degradation of Materials in Nuclear Power Systems-Water Reactors, F. P. Ford, S. M. Bruemmer, and G. S. Was, eds., The Minerals, Metals, and Materials Society, Warrendale, PA, pp. 217-224, 1999.

57. Magdowski, R., and M. Speidel, "Stress Corrosion Crack Growth of Weld Material Alloy 182 in Simulated PWR Environments," Institute of Metallurgy, Swiss Federal Institute, Internal Report No. 226, Zurich, Jan. 2001.

58. Jacko, R. J., R. E. Gold, G. V. Rao, K. Koyama, and A. Kroes, "Results of Accelerated SCC Testing of Alloy 82, Alloy 182 and Alloy 52M Weld Metals," The Vessel Penetration Inspection, Crack Growth and Repair Conference, Oct. 2, 2003, Gaithersburg, MD, 2003, Vol. 1, pp. 413426.

59. Attanasio, S., J. V. Mullen, J. W. Wuthrich, W. W. Wilkening, and D. S. Morton, "Stress Corrosion Crack Growth Rates (SCCGRs) for Alloy 182 and 82 Welds," The Vessel Penetration Inspection, Crack Growth and Repair Conference, Oct. 2, 2003, Gaithersburg, MD, 2003, Vol. 1, pp. 267296.

60. Brown, C. M., and W. J. Mills, "Effect of Water on Mechanical Properties and Stress Corrosion Behavior of Alloy 600, Alloy 690, EN82H Welds, and EN52 Welds," Corrosion, 55 (2), pp. 173–186, 1999.

61. Mills, W. J., and C. M. Brown, "Stress Corrosion Crack Growth Rates for Alloy 82H Welds in High Temperature Water," Proc. 11th Intl. Conf. on Environmental Degradation of Materials in Nuclear Power Systems-Water Reactors, NACE International, Houston, TX, 2003.

62. Tsutsumi, K., H. Kanasaki, K. Yoshimoto, Y. Nomura, S. Asada, and T. Yonezawa, "SCC Growth Rate of Nickel Based Alloy 132 Weld Metal in PWR Water," Proc. 11th Intl. Conf. on Environmental Degradation of Materials in Nuclear Power Systems-Water Reactors, NACE International, Houston, TX, 2003.

63. Frary, M., and C.A. Schuh, Connectivity and percolation behaviour of grain boundary networks in three dimensions, Phil.Mag. A 85 (11), pp. 1123–1143, April 2005.

64. Morton, D. S., S. A. Attanasio, and G. A. Young, "Primary Water SCC Understanding and Chraracterization through Fundamental Testing in the Vicinity of the Nickel/Nickel Oxide Phase Transition," Proc. Tenth Intl. Conf. on Environmental Degradation of Materials in Nuclear Power Systems-Water Reactors, NACE International, Houston, TX, 2001.

65. Lidar, P., M. Konig, J. Engstrom, and K. Gott, "Effect of Water Chemistry on Environmentally Assisted Cracking in Alloy 600 in Simulated PWR Environments," Proc. Ninth International Symposium on Environmental Degradation of Materials in Nuclear Power Systems—Water Reactors, The Minerals, Metals, and Materials Society (TMS), Warrendale, PA, pp. 125–130, 1999.

66. Johnson, L. G., "The Median Ranks of Sample Values in Their Population with an Application to Certain Fatigue Studies," Ind. Math, 2, pp. 1–9, 1951.

67. Lipson, C., and N. J. Sheth, "Statistical Design and Analysis of Engineering Experiments," McGraw Hill, New York, 1973.

68. Beck, J., and K. Arnold, "Parameter Estimation in Engineering and Science," J. Wiley, New York, 1977.

69. Hogg, R. V., and A. T. Craig, "Introduction to Mathematical Statistics," Prentice Hall, New York, 1995.

NRC FORM 335
(2–89)
NRCM 1102,
3201, 3202

U. S. NUCLEAR REGULATORY COMMISSION

BIBLIOGRAPHIC DATA SHEET

(See instructions on the reverse)

1. REPORT NUMBER
(Assigned by NRC. Add Vol., Supp., Rev., and Addendum Numbers, if any.)

NUREG/CR–6907
ANL–04/3

2. TITLE AND SUBTITLE

Crack Growth Rates of Nickel Alloy Welds in a PWR Environment

3. DATE REPORT PUBLISHED

MONTH	YEAR
May	2006

4. FIN OR GRANT NUMBER

Y6388

5. AUTHOR(S)

B. Alexandreanu, O. K. Chopra, and W. J. Shack

6. TYPE OF REPORT

Technical

7. PERIOD COVERED (Inclusive Dates)

8. PERFORMING ORGANIZATION – NAME AND ADDRESS (If NRC, provide Division, Office or Region, U.S. Nuclear Regulatory Commission, and mailing address; if contractor, provide name and mailing address.)

Argonne National Laboratory
9700 South Cass Avenue
Argonne, IL 60439

9. SPONSORING ORGANIZATION – NAME AND ADDRESS *(If NRC, type "Same as above": if contractor, provide NRC Division, Office or Region, U.S. Nuclear Regulatory Commission, and mailing address.)*

Division of Fuel, Engineering and Radiological Research
Office of Nuclear Regulatory Research
U.S. Nuclear Regulatory Commission
Washington, DC 20555–0001

10. SUPPLEMENTARY NOTES

William H. Cullen, Jr., NRC Project Manager

11. ABSTRACT (200 words or less)

Reactor vessel internal components made of nickel–base alloys are susceptible to stress corrosion cracking (SCC). A program is being conducted at Argonne National Laboratory to evaluate the resistance of Ni–alloys and their welds to SCC in simulated LWR coolant environments. This report presents crack growth rate (CGR) results for Alloy 182 in simulated PWR environments. The results indicate little or no environmental enhancement of fatigue CGRs of Alloy 182 weld–metal. In addition, the cyclic CGRs of Alloy 182 ware found to be a factor of ≈5 higher than of Alloy 600 in air under the same loading conditions. The SCC CGRs for weld alloy were close to the average behavior of Alloy 600. The sample orientation was found to have a profound effect on the magnitude of crack growth: cracking was found to propagate faster along the dendrites than across them. The existing CGR data for Ni–alloy weld metals have been compiled and evaluated to establish the effects of key material, loading, and environmental parameters on CGRs in PWR environments. The results from the present study are compared with the existing CGR data for Ni–alloy welds to determine the relative susceptibility of the specific Ni–alloy weld to environmentally enhanced cracking.

12. KEY WORDS/DESCRIPTORS *(List words or phrases that will assist researchers in locating this report.)*

Crack Growth Rate
Ni-base welds
PWR Environment

13. AVAILABILITY STATEMENT

Unlimited

14. SECURITY CLASSIFICATION

(This Page)

Unclassified

(This Report)

Unclassified

15. NUMBER OF PAGES

16.ICE PR

NRC FORM 335 (2–89)